Human Molecular Genetics, 2003, Vol. 12, No. 2 **87–98**
DOI: 10.1093/hmg/ddg014

Disruption of *scribble* (*Scrb1*) causes severe neural tube defects in the *circletail* mouse

Jennifer N. Murdoch[1,*,†], Deborah J. Henderson[2], Kit Doudney[3], Carles Gaston-Massuet[1], Helen M. Phillips[2], Caroline Paternotte[1], Ruth Arkell[4], Philip Stanier[3] and Andrew J. Copp[1]

[1]Neural Development Unit, Institute of Child Health, University College London, 30 Guilford Street, London WC1N 1EH, UK, [2]Institute of Human Genetics, University of Newcastle upon Tyne, International Centre for Life, Newcastle upon Tyne NE1 3BZ, UK, [3]Department of Obstetrics and Gynaecology, Institute of Reproductive and Developmental Biology, Imperial College School of Medicine, London W12 0NN, UK and [4]MRC Mammalian Genetics Unit, Harwell, Oxon OX11 0RD, UK

Received August 23, 2002; Revised and Accepted November 11, 2002

Circletail **is one of only two mouse mutants that exhibit the most severe form of neural tube defect (NTD), termed craniorachischisis. In this disorder, almost the entire brain and spinal cord is affected, owing to a failure to initiate neural tube closure. Craniorachischisis is a significant cause of lethality in humans, yet the molecular mechanisms involved remain poorly understood. Here, we report the identification of the gene mutated in *circletail* (*Crc*), using a positional cloning approach. This gene, *Scrb1*, encodes a member of the LAP protein family related to *Drosophila* scribble, with 16 leucine rich repeats and four PDZ domains. The *Crc* mutant contains a single base insertion that creates a frame shift and leads to premature termination of the Scrb1 protein. We report the expression pattern of *Scrb1* during embryonic and fetal development, and show that *Scrb1* expression closely mirrors the phenotypic defects observed in *Crc/Crc* mutants. In addition, *circletail* genetically interacts with the *loop-tail* mutant, and we reveal overlapping expression of *Scrb1* with *Vangl2*, the gene mutated in *loop-tail*. The identification of the *Crc* gene further defines the nature of the genetic pathway required for the initiation of neural tube closure and provides an important new candidate that may be implicated in the aetiology of human NTDs.**

INTRODUCTION

The neural tube is the embryonic precursor of the brain and spinal cord, and is formed by the rolling up of a flat layer of ectodermal cells (the neural plate) to create a tube. In the mammalian embryo, initiation of neural tube closure occurs at three sites along the body axis (1). The first site of *de novo* closure (so-called Closure 1) occurs in the future cervical region, while the second and third sites of *de novo* closure (Closures 2 and 3) occur at about the forebrain–midbrain boundary, and at the most rostral extent of the forebrain, respectively (1). Closure between these three sites is responsible for the formation of the cranial neural tube, while continuation of closure caudally from the site of Closure 1 is necessary for the formation of the spinal cord.

Disruption of neural tube closure leads to a group of disorders termed neural tube defects (NTDs), which are one of the commonest causes of congenital malformation. NTDs affect around 1 in 1000 pregnancies and are either severely disabling or lethal (2). Neural tube defects are classified according to the region of the body axis that is affected (3). Anencephaly is the consequence of a failure to complete neural tube closure in the brain, whereas spina bifida results from disruption of neural tube closure in the lower spine. The most severe form of NTD is craniorachischisis, in which almost the entire brain and spinal cord remain open. Craniorachischisis is caused by a failure to initiate neural tube formation at Closure 1, at the start of neurulation (3). Craniorachischisis comprises 10–20% of human NTDs (4–6) and is invariably lethal, yet the molecular mechanisms involved are poorly understood.

The estimated recurrence risk of NTD with one affected sibling is 2–5% and this increases to 16% with two affected siblings, revealing a strong genetic predisposition for NTD in humans (7). However, direct analysis of the molecular basis of human NTDs is difficult, owing to the practical and ethical constraints of studying human embryos early in development, and the lack of suitable families available for linkage analysis. In contrast, the mouse provides an excellent model system with which to identify the molecular mechanisms involved in neural tube closure. Indeed, there are over 60 existing mouse mutants

*To whom correspondence should be addressed. Tel: +44 1235834393, ext 361; Fax: +44 1235834776; Email: j.murdoch@har.mrc.ac.uk
†Present address: MRC Mammalian Genetics Unit, Harwell, Oxon OX11 0RD, UK.

that exhibit defects in neurulation resulting in, predominantly, spina bifida or anencephaly (8). Identification of the molecular mechanisms involved in craniorachischisis currently relies solely on two mutants that exhibit a failure of Closure 1: *loop-tail* (*Lp*) and *circletail* (*Crc*). These mutants are essential to our understanding of the molecular mechanisms involved in the initiation of neural tube closure.

Homozygous *Lp/Lp* embryos and homozygous *Crc/Crc* mutants both exhibit failure of initiation of neural tube closure in the future cervical region of the embryo (Closure 1), at E8.5. Consequently, these mutants exhibit a neural tube that remains open from the midbrain/hindbrain boundary throughout the spine (Fig. 1A–C) (9–11), closely modelling the human condition of craniorachischisis. We, and others, recently identified the gene mutated in *loop-tail* as *Vangl2* (formerly known as *Lpp1* or *Ltap*) (12,13). *Vangl2* encodes a protein related to *Drosophila* van gogh/strabismus, with four transmembrane domains and a putative carboxy terminal PDZ-binding motif (12,13). Disruption of *Drosophila strabismus* reveals an essential role for this gene in the establishment of planar cell polarity (PCP), also known as epithelial polarity or tissue polarity (14–16). PCP is evident in a number of tissues in *Drosophila*, such as the regular arrangement of ommatidia in the eye, the formation and directionality of hairs in the wing, and the arrangement of sensory bristles in the thorax. In the *strabismus* mutant, this regular arrangement is lost (14–16). Other genes known to be involved in the establishment of PCP in these tissues include *frizzled*, *dishevelled*, *prickle*, *flamingo*, *rhoA* and the *JNK* cascade (17–19). The involvement of frizzled and dishevelled reveals molecular overlap with the Wnt signalling pathway, for which frizzled is the receptor, and dishevelled a downstream cytoplasmic factor. However, PCP appears not to involve the other downstream components of the canonical Wnt pathway, such as armadillo (β-catenin). Rather, planar cell polarity is mediated by a non-canonical Wnt signalling pathway.

Homologues of all the *Drosophila* PCP pathway genes exist in vertebrates, and much recent evidence implicates the vertebrate PCP pathway in the regulation of the convergent extension cell movements that occur during gastrulation and neurulation. For instance, disruption of the *Xenopus* or zebrafish homologues of *van gogh/strabismus* results in failure of convergent extension, and subsequently to failure of neural tube closure (20–23), while mutation of the JNK genes also affects convergent extension (24). A defect in convergent extension may underlie the failure of neural tube closure in the mouse *loop-tail* mutant.

The *circletail* mouse is the only other reported mutant that exhibits failure of Closure 1. We have shown previously that *Lp* and *Crc* map to different chromosomes (1,15) and so are not allelic (25–27). However, *Crc* and *Lp* exhibit a genetic interaction, such that double heterozygotes (*Lp*/+, *Crc*/+) also exhibit craniorachischisis (25). This reveals that *Crc* and *Lp* act either in the same developmental pathway, or in converging pathways, that is/are essential for the initiation of neural tube closure.

Here, we report the identification of the gene mutated in *Crc*, using a positional cloning approach. We show that this gene, *Scrb1*, exhibits a dynamic pattern of expression that corresponds closely to the range of phenotypic defects observed in *Crc/Crc* fetuses. *Scrb1* encodes a putative cytoplasmic protein with four PDZ domains, leading us to speculate that the Scrb1 protein may directly interact with Vangl2, which carries a PDZ binding domain. In support of this hypothesis, we show that *Scrb1* and *Vangl2* exhibit overlapping expression domains in the mid-gestation embryo. Scrb1 is homologous to the *Drosophila* protein scribble, which has not been implicated in planar cell polarity but is involved in apical–basal polarity.

RESULTS

Scrb1 is mutated in the *circletail* mouse mutant

We previously mapped the *Crc* mutation to an 8.8 cM interval on mouse Chromosome 15, between *D15Mit93* and *D15Mit68* (25). Examination of the publicly available mouse genomic sequence information (see www.ensembl.org/Mus_musculus/) identified over 100 transcripts in the 9 Mb interval between *D15Mit144* (the next most proximal marker to *D15Mit93*) and *D15Mit68.* Several of the genes within the critical region appeared to be good candidates for *circletail.* However, one transcript, Q922S3, appeared to be a particularly striking candidate, since it encodes four PDZ domains and is, therefore, a possible interacting partner for the PDZ-binding domain protein encoded by *Vangl2*, the gene mutated in *loop-tail* (12,13).

Q922S3 proved to be identical to mouse *scribble* (GenBank accession number, AF441233; renamed *Scrb1*) and sequence analysis of the coding region revealed a single base insertion in the *Crc* mutant (3182-3183insC, codon 947), compared with wild-type DNA (Fig. 1E and F). The insertion is unique to the *Crc* mutant, and is absent from 16 other mouse strains, including the parental strains on which *Crc* arose, BALB/C, C57BL/6 and NMRI (11), and the unrelated strains, CBA/Ca, 129/Ola, 129/Sv, A/WySnJ, AKR, BXSB, C57BLKS/J, DBA/2, MRL, NOD, NZB, SJL/J and *Mus spretus.* The insertion causes a frame shift resulting in a premature termination codon and truncation of the protein to 971 amino acids (Fig. 1G and Fig. 2).

Genomic organization and alternative splicing of mouse *Scrb1*, which encodes a member of the LAP protein family

Comparison of genomic and cDNA sequences reveals that mouse *Scrb1* contains 38 exons, ranging in size from 38 to 502 bp, and spans a genomic interval of 22.6 kb (Fig. 1H and Table 1). EST database searches and reverse transcriptase (RT)–PCR reveal several alternative transcripts, with inclusion or exclusion of exons 16, 29 or 36 (Fig. 1I–K). The full length transcript of mouse *Scrb1* is 5547 bp and encodes a putative protein of 1665 amino acids, which exhibits 88% identity with human SCRB1, 44% identity with *Drosophila* Scribble (Fig. 2) and 36% identity with *C.elegans* protein LET-413 (AJ276590, not shown). Scrb1 is a LAP protein, with 16 leucine rich repeats (LRRs) and four predicted PDZ domains (Fig. 1G), two of which are lost from the truncated *Crc* protein (Fig. 1G). In the alternative transcripts, exclusion of exons 16, 29 or 36 is predicted to shorten the protein by 21, 28 or 25 amino acids, respectively, although all putative peptides retain the LRRs and PDZ domains (Fig. 2). Alternative splicing of human *SCRB1*

Table 1. Exon–intron organization of mouse *Scrb1*

Exon number	Exon size (bp)	Intron size (bp)
1	502	1450
2	118	105
3	79	97
4	90	88
5	57	87
6	64	99
7	75	65
8	145	401
9	119	771
10	200	73
11	167	82
12	131	95
13	126	700
14	165	543
15	378	868
16	63	515
17	90	489
18	78	760
19	324	104
20	81	78
21	258	825
22	111	87
23	294	69
24	189	5522
25	111	76
26	57	144
27	75	1288
28	63	509
29	84	157
30	99	109
31	160	76
32	148	82
33	186	77
34	143	69
35	38	118
36	75	249
37	52	83
38	352	
Total	5547	17 010

has not been reported and is not evident from EST database searches although, interestingly, the human transcript contains the region of mouse exon 16 but lacks exons 29 and 36, corresponding to the most abundant variant observed in mouse (Figs. 1I–K and 2). *Drosophila scribble* also demonstrates alternative splicing (28), but differs in genomic organization and yields transcripts that are distinct from those in mouse (28).

Scrb1 is expressed in the neuroepithelium and several additional tissues showing abnormalities in *Crc* mutants

In situ hybridization experiments performed with sense probes show no staining (Fig. 3A and H, cf. B, C and I–T), whereas antisense probes reveal robust staining in a variety of tissues during embryonic and fetal development (Fig. 3B–G, I–S). *Scrb1* is expressed from at least embryonic day (E) 7.5 (not shown) and, at the time of initiation of neural tube closure, the most intense expression is detected in the neuroepithelium (Fig. 3B–G). This suggests that the defect in neurulation may be intrinsic to the neural plate. Less intense expression is also detected, at this stage, in the cranial mesenchyme and branchial arches (Fig. 3D and E) and low intensity expression is seen in the somitic mesoderm (Fig. 3F) and, more caudally, in the lateral mesoderm (Fig. 3G). The expression of *Scrb1* appears to correlate closely with the mutant phenotype in *Crc*. For instance, expression in the developing somites correlates with the observation of somite disorganization in *Crc/Crc* embryos (Fig. 1D). *Scrb1* is also observed in the developing heart (Fig. 3I), in correlation with the severe cardiac defects seen in *Crc* mutants (D.J. Henderson *et al.*, manuscript in preparation), and in the hepatic primordium (Fig. 3J), which appears overgrown in *Crc/Crc* fetuses (Fig. 1A and data not shown). In addition, expression in the lateral mesoderm of the future body wall (Fig. 3G and J and data not shown), may contribute to the failure of abdominal closure in *Crc/Crc* fetuses (Fig. 1A).

During later developmental stages, *Scrb1* is expressed in the eyelid epithelium, particularly at the region of eyelid fusion, and in the retina (Fig. 3K and L). These expression domains correlate with the failure of *Crc/Crc* fetuses to form closed eyelids (Fig. 4A and B) and with the partially penetrant defects observed in the retina (11). *Scrb1* is also expressed in the submandibular glands (Fig. 3O), which exhibit reduced branching in *Crc* mutants (Fig. 4C and D). The whisker and hair follicles also express *Scrb1* (Fig. 3M and N), and these structures appear small in *Crc/Crc* fetuses (Fig. 4E and F) (data not shown). Expression is also evident in the sympathetic ganglia (Fig. 3P), which are hypoplastic in *Crc/Crc* (Fig. 4G and H), and in the developing inner ear (Fig. 3R), which is abnormal in *Crc/Crc* fetuses (data not shown).

Scrb1 expression is evident in a number of other fetal tissues, including the thymus, testis, kidney, the epithelial lining of the oesophagus and stomach, the trigeminal and dorsal root ganglia, and the lung epithelia (Fig. 3P, Q, S and T), although no gross abnormalities have so far been detected in these tissues in *Crc/Crc* mutants. Thus, *Scrb1* expression is detected in all of the tissues in which a morphological phenotype has been detected, although not all sites of *Scrb1* expression exhibit a mutant phenotype, perhaps suggesting redundancy with other co-expressed genes.

Scrb1 expression domains overlap with *Vangl2*, a putative interacting partner

We have shown previously that the *circletail* mutant exhibits a genetic interaction with the *loop-tail* mutant, such that double heterozygotes (*Crc*/+, *Lp*/+) exhibit severe neural tube defects, very similar to the phenotype of individual *Crc/Crc* or *Lp/Lp* homozygotes (25). This genetic interaction suggests a molecular interaction between Scrb1 and Vangl2, the proteins mutated in *Crc* and *Lp*. Comparison of *Scrb1* and *Vangl2* expression patterns reveals that many embryonic and fetal tissues co-express both genes, including the neuroepithelium, ventricular myocardium, eyelids, lung epithelium, whisker follicles and the epithelial lining of the stomach (Fig. 3I, L, N, Q and T–W) (12, and data not shown). This co-expression further supports the hypothesis that the proteins may directly interact. Furthermore, histological analysis of *Crc/Crc* embryos just at the stage of initiation of neural tube closure reveals an

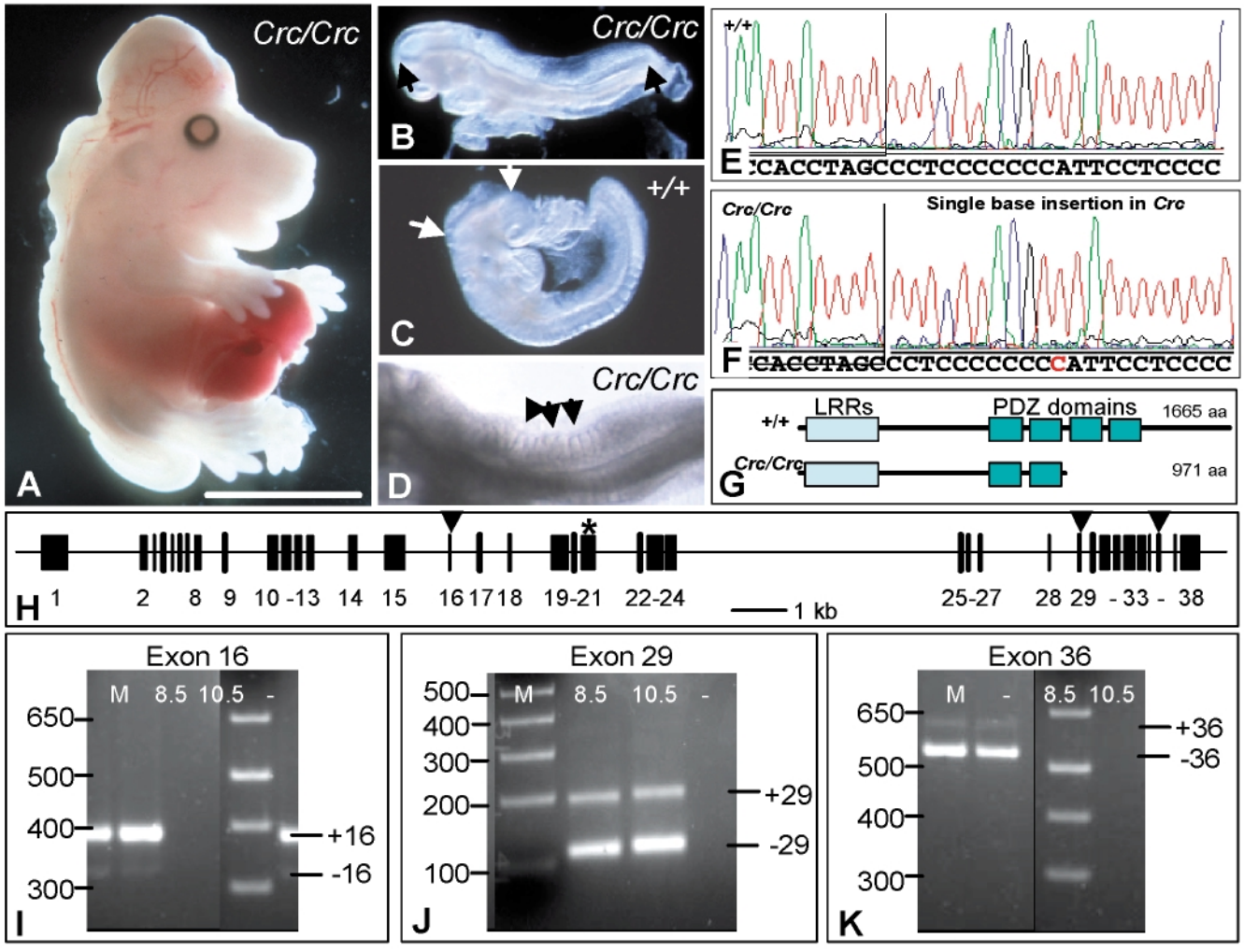

Figure 1. Mutation of the *Scrb1* gene in the *circletail* mutant. (**A**) *Crc/Crc* fetuses exhibit an open neural tube from the midbrain throughout the spine, and also exhibit gastroschisis, with protrusion of the liver from the abdominal cavity. (**B**, **C**) The severe neural tube defect in *Crc/Crc* is caused by a failure to initiate neural tube closure at E8.5 (B, cf. C). The neural tube remains open from the midbrain to the tail bud in *Crc/Crc* (B, between arrows) while only the cranial neural tube is open in the +/+ littermate at this stage (C). *Crc/Crc* embryos also exhibit delayed and incomplete axial rotation (B, cf. C), which may contribute to the gastroschisis. (**D**) Higher power view of *Crc/Crc* embryo in B showing irregular segmentation of somites (arrows). (**E**, **F**) Comparative sequencing of the *Scrb1* gene in +/+ (E) and *Crc/Crc* (F) cDNA identified a single base insertion in *Crc/Crc* (arrow, F). (**G**) Schematic diagram of Scrb1 protein, with 1665 amino acids encoding 16 leucine-rich repeats (LRRs) and four PDZ domains in wild-type. In *Crc*, the insertion causes a frameshift which leads to truncation of the Scrb1 peptide to 971 amino acids with the loss of two PDZ domains. (**H**) Genomic organization of mouse *Scrb1*, with 38 exons (solid boxes) over 23 kb genomic DNA. The *Crc* mutation occurs in exon 21 (asterisk), while exons 16, 29 and 36 (arrows) are subject to alternative splicing. (**I**–**K**) RT–PCR analysis confirms the alternative splicing of *Scrb1*. At E8.5 and E10.5, the predominant transcripts include exon 16 (I), exclude exon 29 (J) and exclude exon 36 (K). M, molecular weight markers, −, negative controls. Scale bar, 4.0 mm (A), 1.4 mm (B, C) and 0.8 mm (D).

expanded neural plate midline and widened notochord (Fig. 4I and J), very similar to the phenotype of *Lp/Lp* embryos (29) and in keeping with Scrb1 and Vangl2 having a common site of action. Examination of *Scrb1* expression in *Lp/Lp* mutants, and conversely, *Vangl2* expression in *Crc/Crc* mutants, reveals no defect in mRNA localization (Fig. 5A–J), excluding transcriptional regulation as a possible mechanism of interaction between these genes. Rather, since Vangl2 carries a carboxy-terminal PDZ binding domain, while Scrb1 carries four PDZ domains, we hypothesize that the interaction between these proteins may occur in the form of a direct protein–protein interaction.

Circletail mutants exhibit no generalised defect in neuroepithelial apical–basal polarity

Drosophila scribble is involved in regulating apical–basal polarity (30). To test for a generalized loss of apical–basal polarity in *circletail* mutants, we stained sections with fluorescently conjugated phalloidin, which binds to F-actin. During neurulation, actin microfilaments exhibit a marked apical localization in the neuroepithelium, particularly in more cranial regions of the body axis (31). Phalloidin staining of *circletail* mutant embryos both immediately before the onset of neural tube closure, at the five somite stage, and several

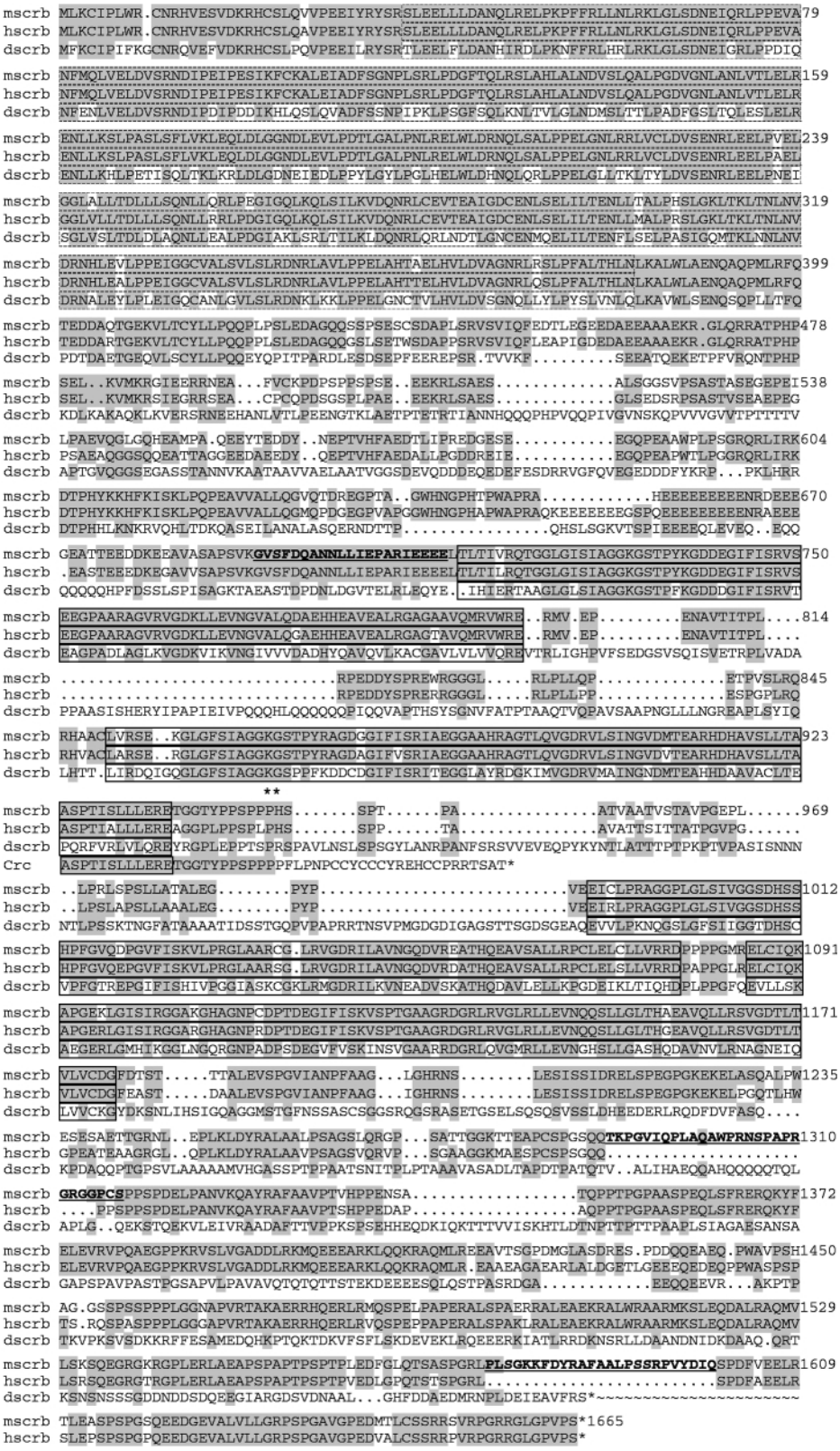

Figure 2. Comparison of peptide sequences of scribble from mouse (mscrb, AA441233), human (hscrb, AY062238) and *Drosophila* (dscrb, AAF26357). Identical amino acids are shaded, and the three alternatively used mouse exons are shown in bold and underlined. The leucine-rich repeats are outlined with a dashed box, and the four PDZ domains are outlined with a solid box. Numbering refers to the mouse peptide. The consequence of the insertion in *Crc* codon 947 is shown as a fourth line of sequence, with the position of the mutation marked (**).

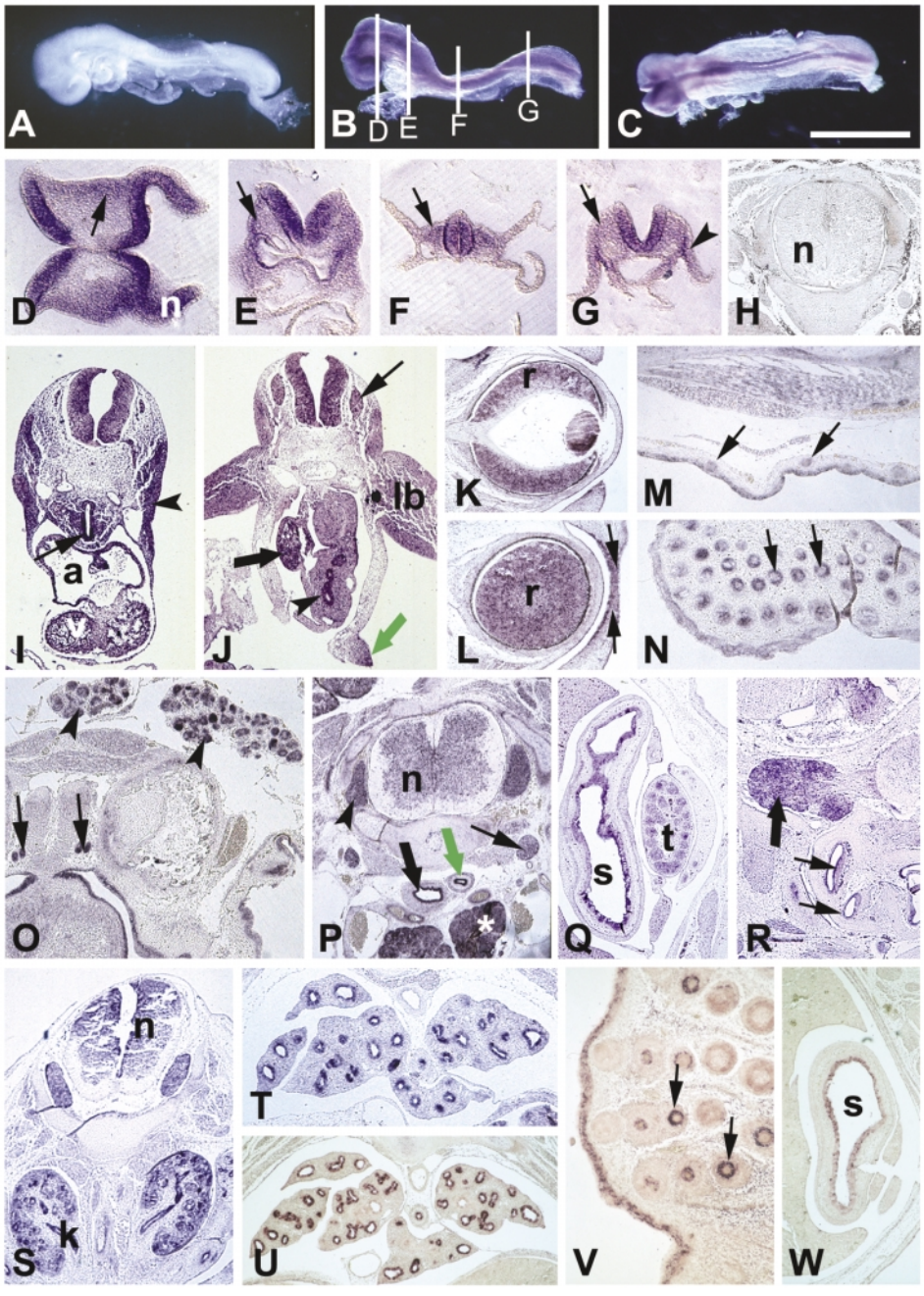

Figure 3. Embryonic and fetal expression of *Scrb1* shown by *in situ* hybridization, and comparison with *Vangl2* expression. (**A**) Wholemount *in situ* hybridization with sense probe for *Scrb1* at E8.5, showing complete lack of staining. (**B**, **C**) Wholemount *in situ* hybridization with antisense probe for *Scrb1*, showing that *Scrb1* expression extends in a longitudinal domain along the length of the embryo at E8.5 (B, lateral and C, dorsal views). (**D–G**) Transverse sections through the embryo shown in B show that at E8.5 expression is most intense within the neuroepithelium, but detectable at lower intensity within the cranial mesenchyme (arrow, D), branchial arches (arrow, E), somitic and presomitic mesoderm (arrows, F and G) and lateral mesoderm (arrowhead, G). (**H**) Slide *in situ* hybridization with the *Scrb1* sense probe shows only a low level of background staining. (**I**, **J**) Slide *in situ* hybridization with antisense *Scrb1* probe at E10.5 reveals continued *Scrb1* expression in the branchial arches (arrowhead, I) and neural tube (I, J), while expression is also apparent in the developing heart (I), trachea (arrow, I), limb buds (J), dorsal root ganglia (thin arrow, J), midgut epithelium (arrowhead, J), medial body wall (open arrow, J) and in the liver primordium (thick arrow, J). (**K–P**) At E15.5, intense *Scrb1* expression is apparent in the retina (K, L) and in the epithelium of the developing eyelids, particularly at the region of eyelid fusion (arrows, L). *Scrb1* expression is also detected in the developing hair and whisker follicles (arrows, M and N), and in the submandibular glands (arrowheads, O) and ducts (arrows, O). Further *Scrb1* mRNA is detected in the thymus (asterisk, P), trachea (thick arrow, P), oesophagus (open arrow, P), sympathetic ganglia (thin arrow, P) and in the dorsal root ganglia (arrowhead, P). (**Q**, **R**) Sections in E14.5 fetuses reveal *Scrb1* expression in the testis (Q), epithelial lining of the stomach (Q), trigeminal ganglia (thick arrow, R) and the cochlea (thin arrows, R). (**S**, **T**) At E13.5, *Scrb1* expression is evident in the kidney (S) and in the lung bud epithelium (T). (**U–W**) *Vangl2* expression is shown in the lung epithelium (U), and epithelial lining of the stomach (W) at E14.5, and in the whisker follicles (arrows, V) at E15.5. Abbreviations: a, atria; k, kidney; lb, limb bud; n, neuroepithelium; r, retina; s, stomach; t, testis; v, ventricle; dashed lines in B indicate approximate levels of sections shown in D–G. Sections are either coronal (K, L), sagittal (O, Q, R, V, W) or transverse (H, I, J, M, N, P, S, T, U). Scale bar, 1.0 mm (A–C), 300 μm (D–G, O), 700 μm (H, I, J, P, S), 500 μm (K, L), 400 μm (M, Q, V), and 900 μm (N, R, T, U, W).

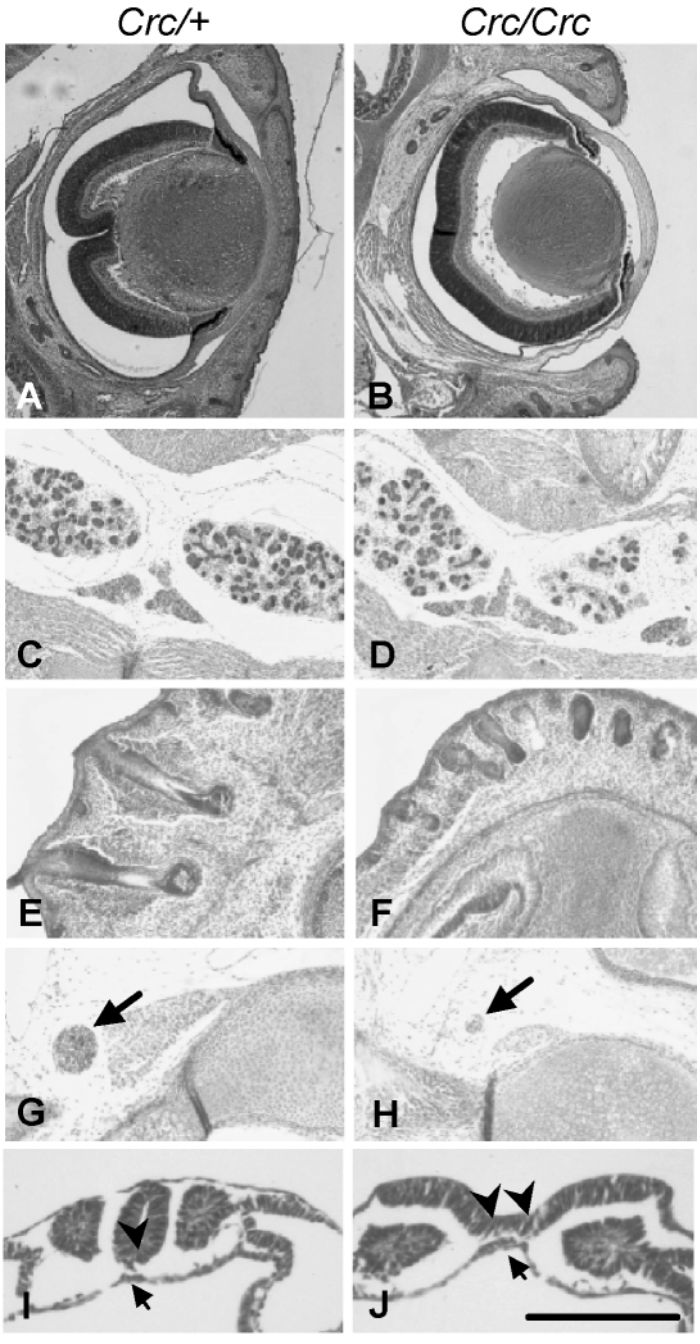

Figure 4. Phenotypic abnormalities in *Crc/Crc* mutants revealed in histological sections stained with haematoxylin and eosin, with comparison of *Crc/Crc* mutants (B, D, F, H, J) and phenotypically normal *Crc*/+ littermates (A, C, E, G, I). (**A, B**) At E18.5, *Crc/Crc* fetuses exhibit failure to form closed eyelids (B, cf. A). The bifurcation of the retina in *a* is an histological artefact. (**C–F**) At E16.5, *Crc/Crc* fetuses exhibit reduced branching in the submandibular glands (D, cf. C) and have whisker follicles that appear small or delayed (F, cf. E). Mutants also have hypoplastic sympathetic ganglia (arrows, H, cf. G). (**I–J**) At the seven somite stage, *Crc*/+ embryos exhibit initiation of neural tube closure (I), with a compact median hinge point in the ventral midline of the neural tube (arrowhead), and a discrete notochord (arrow). In contrast, *Crc/Crc* embryos exhibit complete failure of initiation of neural tube closure at this axial level (J), with widely splayed neural folds and a broadened and flattened midline region flanked by bilateral bending points (arrowheads, J). The notochord is also broadened (thick arrows, J). Scale bar, 800 μm (A, B) 400 μm (C–H) and 120 μm (I, J).

hours after the time of initiation of neural tube closure, at the 16 somite stage, reveals no obvious defect in actin localization in the mutant embryos (Fig. 5M, N, Q and R), compared with heterozygous or wild type littermates (Fig. 5K, L, O and P). This demonstrates that there is no general disruption in apical–basal polarity in the *Crc/Crc* neuroepithelium, although we have not excluded the possibility of disruption of specific apically restricted proteins.

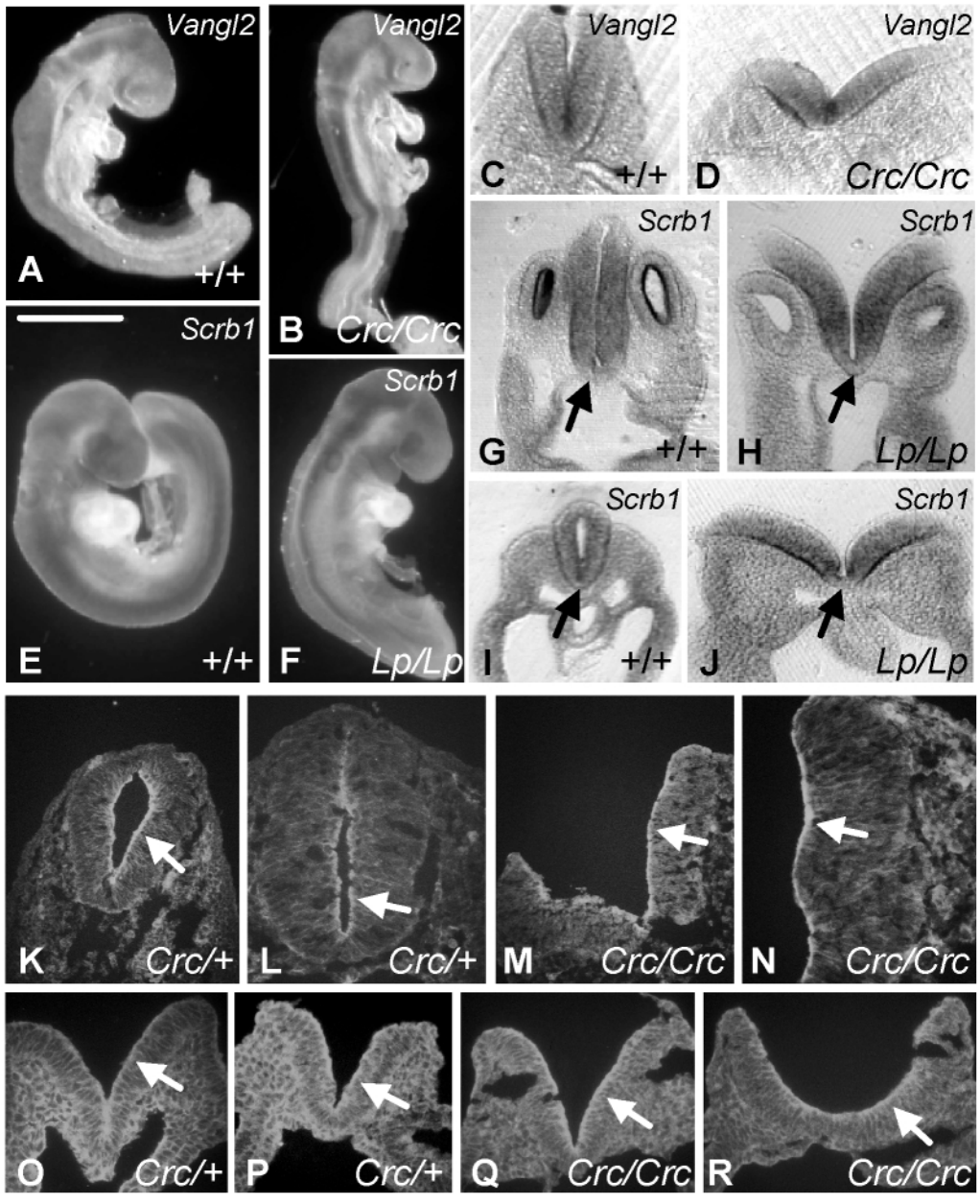

Figure 5. Examination of *Vangl2* expression and actin localization in *Crc/Crc* mutant embryos, and *Scrb1* expression in *Lp/Lp* mutant embryos, and comparison to wild-type littermates. (**A–D**) Wholemount *in situ* hybridization of *Vangl2* on wild-type (A, C) and *Crc/Crc* mutant embryos (B, D) at E8.5 reveals similar expression patterns in whole embryos (A, B) and in transverse sections (C, D), with *Vangl2* expression apparent in the medial region of the neuroepithelium. (**E–J**) Wholemount *in situ* hybridization of *Scrb1* on wild type (E, G, I) and *Lp/Lp* mutant embryos (F, H, J) at E9 reveals similar expression domains in whole embryos (E, F) and in transverse sections (G–J). In these embryos, *Scrb1* expression appears to be reduced or absent from the developing floor plate (arrows, G–J), which is enlarged in the *Lp* mutant. (**K–R**) Phalloidin staining to reveal the distribution of actin in transverse sections through the neuroepithelium of *Crc*/+ and *Crc/Crc* littermates, at 16 somite stage (K–N) and five to six somite stage (O–R). Actin localization appears very similar in homozygous mutant (M, N, Q, R) and heterozygous embryos (K, L, O, P), with very obvious apical restriction at the 16 somite stage (arrows, K–N), and a more widespread distribution but with some apical preference at the five to six somite stage (arrows, O–R). Scale bar, 800 μm (A, B), 150 μm (C, D), 1 mm (E, F), 400 μm (G, H), 200 μm (I, J, K, M), 100 μm (L, N–R).

DISCUSSION

We have identified a frameshift mutation in the *Scrb1* gene as the cause of the craniorachischisis phenotype seen in the *circletail* mouse mutant. *Scrb1* is initially expressed most intensely in the neuroepithelium, suggesting a defect intrinsic to the neural plate. In addition, we have shown that *Scrb1* expression is associated with other regions of phenotypic abnormalities in the *Crc* mutants, including the heart, inner ear, whisker and hair follicles, eyelids, submandibular glands and

the sympathetic ganglia. Indeed, all of the tissues that demonstrate a mutant phenotype in *circletail* also exhibit expression of *Scrb1*. Additionally, *Scrb1* is expressed in a diverse array of other embryonic and fetal tissues including epithelial tissues of neuroectodermal (for example, the cochlea), endodermal (lining of the gut and stomach) and ectodermal (eyelid epithelium) origin, as well as non-epithelial tissues, such as the cranial mesenchyme.

Scrb1 may be involved in the cell movements of convergent extension

The severe neural tube defect exhibited by the *circletail* mutant is seen in only one other mouse mutant, *loop-tail.* Although not yet specifically demonstrated, it is likely that the neurulation defect exhibited by *loop-tail* is caused by a disruption in the cell movements of convergent extension (13), in which cells move towards the midline, enabling anterior–posterior elongation and medio-lateral narrowing of the embryo (32,33). Indeed, *Lp* mutants exhibit a shortened body axis and widened midline, in keeping with such a cellular defect (29,34). Moreover, mis-expression of the homologous genes in *Xenopus* and zebrafish has been clearly demonstrated to cause defects in convergent extension (19–22,24,35).

The *circletail* mutant exhibits several morphological features that are similar to *loop-tail*, suggesting that a defect in convergent extension may underlie the neural tube defect in this mutant. Indeed, *Crc/Crc* embryos are shorter than their wild-type littermates (11) and we show here that they also exhibit a widened, flattened midline, in keeping with a defect in convergent extension. Moreover, intercrosses have shown that compound heterozygous embryos (*Lp*/+, *Crc*/+) also exhibit the severe neural tube defect (25), indicating that the two mutations interact, presumably through effects on the same tissue.

Mammalian Scrb1 is related to *Drosophila* scribble, a protein involved in apical–basal polarity and tight junction formation

Scrb1 encodes a member of the LAP (leucine-rich repeat and PDZ domain) protein family, most closely related to *Drosophila* scribble and *C.elegans* protein LET-413, which perform essential roles in the establishment of cellular apical–basal polarity (30,36). *Drosophila* scribble localizes to epithelial septate junctions, while LET-413 is localized basolaterally, and disruption of either protein results in abnormal adherens junction formation and failure to restrict the localization of specific junctional and apical membrane proteins (30,36). This results in defects in the organization and differentiation of epithelia, with aberrant cell shapes and loss of the monolayer organization of epithelia in the embryo, larval imaginal discs and adult follicles (30,37). These defects become more severe as development proceeds (30), and the abnormal epithelia also show tumour-like overgrowth (37). Mutations in *scribble* were also independently identified in a screen for genes that control the immune response in *Drosophila* (38). The structure of the fat body, the organ responsible for the principle humoral response to infection, is abnormal in *scribble* mutants, with the cells exhibiting a more rounded morphology indicative of abnormal junctional structures (38).

Although the cellular role of mammalian Scrb1 remains to be determined, the similarity to *Drosophila* scribble suggests that this protein may also be involved in apical–basal polarity. Indeed, human scribble partially colocalizes with tight junctions (39), supporting the hypothesis of functional conservation. Furthermore, increased degradation of scribble in human cells, through the ubiquitin-mediated pathway stimulated by the high-risk human papillomavirus E6 proteins, correlates with a disruption in the integrity of tight junctions (39).

Scrb1 is initially expressed most intensely in the neuroepithelium, and the apical–basal polarity of this tissue is known to be tightly regulated during neurulation (40,41). Using phalloidin staining, we have demonstrated that there is no generalized loss of apical–basal polarity in the neuroepithelium of *circletail* mutant embryos. However, it is plausible that disruption of *Scrb1* may lead to loss of the apically restricted localization of a specific subset of apical proteins, analogous to the defect observed in *Drosophila scribble* mutants. Such a specific defect may only become apparent once the targets of mammalian Scrb1 are identified.

The defects observed in other mutant tissues, such as the eyelid, whisker follicles and salivary glands, may also be caused by a disruption in the subcellular distribution of specific apical membrane targets of Scrb1. Alternatively, some of the observed defects may perhaps be caused by alterations in cell proliferation, since *Drosophila scribble* is involved in regulating proliferation (37). It is not yet clear if the mutation of *Scrb1* in *circletail* results in a null phenotype. While truncation of *Scrb1* could destabilize the protein and lead to complete loss of function, it is also possible that the shortened Scrb1 peptide is stable, as seen in *Drosophila* (28) and instead could exhibit dominant-negative activity.

Genetic interaction between *Lp* and *Crc*: possible links of Scrb1 to planar cell polarity

The genetic interaction between *circletail* and *loop-tail* reveals a functional link between Scrb1 and Vangl2, since compound heterozygous mutants exhibit the same severe neural tube defect that is seen in either homozygous mutant (25). Vangl2 is likely to participate in the vertebrate planar cell polarity pathway (14–16,18,19,21,22,42). Although not previously implicated in this pathway, it is possible that Scrb1 may also have some direct function in planar cell polarity, and possible molecular interactions with PCP signalling are discussed below. Alternatively, Scrb1 may affect PCP through an effect on apical–basal polarity. Indeed, correct apical–basal polarity is thought to be essential for the establishment of planar cell polarity, and these processes are closely integrated in the regulation of asymmetric cell division in *Drosophila* (43). A third possibility is that mammalian Scrb1 is not required for either apical–basal or planar cell polarity, but that it functions in a distinct pathway which converges with the PCP pathway to regulate cell movements during early neurulation. Recent evidence suggests that other molecular pathways are important in regulating convergent extension cell movements, including a non-canonical FGF signalling pathway involving the marginal coil protein (44). Intriguingly, Vangl2 may potentially interact

in this pathway, since both marginal coil and Vangl2 contain coiled coil domains (12,44), providing the potential for direct protein interaction. Clearly, much further work is required to decipher the precise functional role of mammalian Scrb1.

Putative molecular interactions between Scrb1 and Vangl2

Although the molecular basis of the genetic interaction between *Crc* and *Lp* is unknown, a number of possibilities exist. We have excluded one hypothesis, that *Crc* and *Lp* may act in a regulatory cascade, since both *Vangl2* and *Scrb1* exhibit apparently normal expression in *Crc/Crc* and *Lp/Lp* mutants, respectively. Another possibility is that Scrb1 may function to control the subcellular localization of the Vangl2 protein. Alternatively, Scrb1 and Vangl2 may form part of a protein complex, perhaps through direct interaction of the carboxy-terminal PDZ-binding motif (PBM) of Vangl2 with the PDZ domains of Scrb1. The *Xenopus* Vangl2 homologue has been shown to bind to the PDZ domains of dishevelled although, surprisingly, the PBM of Vangl2 was not required for this interaction (20). The PBM of Vangl2 appears to be essential in regulating cell polarity and driving convergent extension (20,23), suggesting that interaction of the PBM of Vangl2 with a PDZ protein other than dishevelled may be functionally important. Another hypothesis is that Scrb1 may act downstream of Vangl2 in the PCP pathway. The leucine-rich repeats of Scrb1 are similar to those found in other proteins that are known to interact with proteins of the small GTPase family (45,46). This raises the possibility that there may be an interaction between the Scrb1 LRRs and RhoA, a small GTPase that acts downstream in the PCP pathway (17). Distinguishing between these possibilities requires the development of mouse-reactive anti-Vangl2 and anti-Scrb1 antibodies, and these will be the subject of future work. Moreover, the presence of four PDZ domains and 16 LRRs provides the potential for Scrb1 to exhibit multiple protein–protein interactions, with the ability to form a multiprotein complex that could be essential in linking apical–basal polarity or other signalling pathways with planar cell polarity in mammalian development.

Relevance to human disease

Despite numerous studies, the identity of the genes involved in human NTD has remained elusive (47). Whilst the mRNA and predicted protein sequences of human *SCRB1* are available, this gene has not been formally mapped and is not yet annotated in the publicly available human genome sequence databases, presumably as it lies within a region that is incompletely sequenced. However, numerous genes that closely flank *Scrb1* on mouse Chromosome 15 have homologues on human Chromosome 8q24, including *Ly6h* and *Grbp* (*Rhophilin1*) proximally, and *Plectin*1, *Hsf*1 and *Dgat*1, distally. Thus, it seems very likely that human *SCRB1* will also localize to this region. In support of this prediction, BLAST homology searches of the high throughput genomic sequence database with the human *SCRB1* cDNA sequence identifies perfect matches in two genomic clones which have been used for low-pass sequence sampling, BACs RP11-299N14 and RP11-429J17, and a fragment from one end of clone RP11-299N14 has been localized to 8q24, in the human genomic sequence database (http://genome.cse.ucsc.edu/).

Although, to our knowledge, chromosome 8q24 has not previously been associated with human NTDs, *Scrb1* represents an important new candidate for this severe congenital defect. The complex aetiology and low penetrance of NTD in humans is suggestive of a polygenic and multifactorial mode of inheritance. The severe neural tube defects demonstrated by *Lp*/+, *Crc*/+ double heterozygotes show that mutations in two different genes can act in synergy to generate a severe phenotype. In humans, there are now numerous examples where birth defects result from double heterozygous mutations that act synergistically, including holoprosencephaly (*SHH* and *TGIF*) (48), retinitis pigmentosa (*ROM1* and *RDS*) (49) and Bardet–Bidel syndrome (*BBS2* and *BBS6*) (50). Despite a general lack of success at identifying causative mutations in human orthologues of mouse NTD genes, an approach that looks at multiple interacting genes, perhaps in specific biochemical pathways, may be more fruitful. The identification of *Scrb1* and its interaction with *Vangl2* suggests an important new candidate for NTDs in human patients.

MATERIALS AND METHODS

Mouse strains BALB/c, CBA/Ca, C57BL/6J, 129/Ola and 129/Sv were obtained from Harlan Olac (Bicester, UK); NMRI was obtained from NIH; and A/WySnJ, AKR, BXSB, C57BLKS/J, DBA/2, MRL, *Mus spretus*, NOD, NZB and SJL/J were obtained from the Jackson Laboratories (Bar Harbor, ME, USA). Mice carrying the *Lp* mutation were bred and genotyped as described previously (12,51). Mice carrying the *Crc* mutation were maintained as described previously (25), and embryos were genotyped at *D15Mit144* and *D15Mit68.* Embryos were harvested and processed for histology or *in situ* hybridization as described elsewhere (52). Sense and antisense probes for *Scrb1* were generated by transcription of a 770 bp fragment, corresponding to cDNA region 541–1310 bp, cloned into the pGEM-T (Promega) vector. The antisense probe detects all possible splice variants, and sense probes gave no staining above background.

RNA extraction and reverse transcription was performed as described (12). Analysis of alternative splicing of exons 16, 29 and 36 was performed by RT–PCR using primers designed in flanking exons, and band identities were confirmed by sequencing.

Comparative sequence analysis of coding exons in *Crc/Crc* and wild-type mice was performed by direct sequencing of PCR-amplified products generated with specific primers designed within exons (for cDNA analysis) or flanking exons (for genomic DNA analysis). Sequencing reactions were analysed with a MegaBACE1000 automated sequencer (Amersham). BLAST searches were performed using the NCBI web server (http://www.ncbi.nlm.nih.gov/blast), and protein structure was analysed using the PIX package (available at the HGMP Resource Centre, Hinxton, UK).

Histological analysis was performed on embryos or fetuses embedded in paraffin wax, using standard protocols. Sections were stained with haematoxylin and eosin. Phalloidin staining was performed on sections of frozen tissue, using FITC-phalloidin (Sigma) as described previously (31).

ACKNOWLEDGEMENTS

We thank Nicholas Greene for critical reading of the manuscript and Terry Hacker for assistance with histology. This work was supported by grants from the Medical Research Council, British Heart Foundation, Wellcome Trust, SPARKS, the Welton Foundation, European Union and Birth Defects Foundation.

REFERENCES

1. Copp, A.J., Brook, F.A., Estibeiro, J.P., Shum, A.S.W. and Cockroft, D.L. (1990) The embryonic development of mammalian neural tube defects. *Prog. Neurobiol.*, **35**, 363–403.
2. Copp, A.J. and Bernfield, M. (1994) Etiology and pathogenesis of human neural tube defects: insights from mouse models. *Curr. Opin. Pediatr.*, **6**, 624–631.
3. Harding, B.N. and Copp, A.J. (2002) In Graham, D.I. and Lantos, P.L. (eds), *Greenfield's Neuropathology.* Arnold, London, Vol. 1, pp. 357–483.
4. Seller, M.J. (1987) Neural tube defects and sex ratios. *Am. J. Med. Genet.*, **26**, 699–707.
5. Berry, R.J., Li, Z., Erickson, J.D., Li, S., Moore, C.A., Wang, H., Mulinare, J., Zhao, P., Wong, L.Y.C., Gindler, J., Hong, S.X., Correa, A. and China–US Collaborative Project NEU (1999) Prevention of neural-tube defects with folic acid in China. *New Engl. J. Med.*, **341**, 1485–1490.
6. Kirillova, I., Novikova, I., Aug J., Audollent, S., Esnault, D., Encha-Razavi, F., Lazjuk, G., Atti-Bitach, T. and Vekemans, M. (2000) Expression of the sonic hedgehog gene in human embryos with neural tube defects. *Teratology*, **61**, 347–354.
7. Lalouel, J.M., Morton, N.E. and Jackson, J. (1979) Neural tube malformations: Complex segregation analysis and calculation of recurrence risks. *J. Med. Genet.*, **16**, 8–13.
8. Juriloff, D.M. and Harris, M.J. (2000) Mouse models for neural tube closure defects. *Hum. Mol. Genet.*, **9**, 993–1000.
9. Copp, A.J., Checiu, I. and Henson, J.N. (1994) Developmental basis of severe neural tube defects in the *loop-tail* (*Lp*) mutant mouse: use of microsatellite DNA markers to identify embryonic genotype. *Devl. Biol.*, **165**, 20–29.
10. Gerrelli, D. and Copp, A.J. (1997) Failure of neural tube closure in the *loop-tail* (*Lp*) mutant mouse: analysis of the embryonic mechanism. *Devl. Brain Res.*, **102**, 217–224.
11. Rachel, R.A., Murdoch, J.N., Beermann, F., Copp, A.J. and Mason, C.A. (2000) Retinal axon misrouting at the optic chiasm in mice with neural tube closure defects. *Devl. Genet.*, **27**, 32–47.
12. Murdoch, J.N., Doudney, K., Paternotte, C., Copp, A.J. and Stanier, P. (2001) Severe neural tube defects in the loop-tail mouse result from mutation of Lpp1, a novel gene involved in floor plate specification. *Hum. Mol. Genet.*, **10**, 2593–2601.
13. Kibar, Z., Vogan, K.J., Groulx, N., Justice, M.J., Underhill, D.A. and Gros, P. (2001) Ltap, a mammalian homolog of *Drosophila* Strabismus/Van Gogh, is altered in the mouse neural tube mutant Loop-tail. *Nat. Genet.*, **28**, 251–255.
14. Wolff, T. and Rubin, G.M. (1998) Strabismus, a novel gene that regulates tissue polarity and cell fate decisions in Drosophila. *Development*, **125**, 1149–1159.
15. Taylor, J., Abramova, N., Charlton, J. and Adler, P.N. (1998) Van Gogh: a new *Drosophila* tissue polarity gene. *Genetics*, **150**, 199–210.
16. Adler, P.N., Taylor, J. and Charlton, J. (2000) The domineering non-autonomy of *frizzled* and *Van Gogh* clones in the *Drosophila* wing is a consequence of a disruption in local signaling. *Mech. Devl.*, **96**, 197–207.
17. Shulman, J.M., Perrimon, N. and Axelrod, J.D. (1998) Frizzled signaling and the developmental control of cell polarity. *Trends Genet.*, **14**, 452–458.
18. Adler, P.N. and Lee, H. (2001) Frizzled signaling and cell–cell interactions in planar polarity. *Curr. Opin. Cell Biol.*, **13**, 635–640.
19. Heisenberg, C.-P. and Tada, M. (2002) Wnt signalling: a moving picture emerges from *van gogh*. *Curr. Biol.*, **12**, R126–R128.
20. Park, M. and Moon, R.T. (2002) The planar cell-polarity gene stbm regulates cell behaviour and cell fate in vertebrate embryos. *Nat. Cell Biol.*, **4**, 20–25.
21. Darken, R.S., Scola, A.M., Rakeman, A.S., Das, G., Mlodzik, M. and Wilson, P.A. (2002) The planar polarity gene strabismus regulates convergent extension movements in Xenopus. *EMBO J*, **21**, 976–985.
22. Jessen, J.R., Topczewski, J., Bingham, S., Sepich, D.S., Marlow, F., Chandrasekhar, A. and Solnica-Krezel, L. (2002) Zebrafish *trilobite* identifies new roles for Strabismus in gastrulation and neuronal movements. *Nat. Cell Biol.*, **4**, 610–615.
23. Goto, T. and Keller, R. (2002) The planar cell polarity gene strabismus regulates convergence and extension and neural fold closure in Xenopus. *Devl. Biol.*, **247**, 165–181.
24. Yamanaka, H., Moriguchi, T., Masuyama, N., Kusakabe, M., Hanafusa, H., Takada, R., Takada, S. and Nishida, E. (2002) JNK functions in the non-canonical Wnt pathway to regulate convergent extension movements in vertebrates. *EMBO Rep.*, **3**, 69–75.
25. Murdoch, J.N., Rachel, R.A., Shah, S., Beermann, F., Stanier, P., Mason, C.A. and Copp, A.J. (2001) *Circletail*, a new mouse mutant with severe neural tube defects: chromosomal localization and interaction with the *loop-tail* mutation. *Genomics*, **78**, 55–63.
26. Doudney, K., Murdoch, J.N., Paternotte, C., Bentley, L., Gregory, S., Copp, A.J. and Stanier, P. (2001) Comparative physical and transcript maps of ~1 Mb around loop-tail, a gene for severe neural tube defects on distal mouse chromosome 1 and human chromosome 1q22-q23. *Genomics*, **72**, 180–192.
27. Eddleston, J., Murdoch, J.N., Copp, A.J. and Stanier, P. (1999) Physical and transcriptional map of a three megabase region of mouse Chromosome 1 containing the gene for the neural tube defect mutant *loop-tail* (*Lp*). *Genomics*, **56**, 149–159.
28. Li, M., Marhold, J., Gatos, A., Török, I. and Mechler, B.M. (2001) Differential expression of two scribble isoforms during *Drosophila* embryogenesis. *Mech. Devl.*, **108**, 185–190.
29. Greene, N.D.E., Gerrelli, D., Van Straaten, H.W.M. and Copp, A.J. (1998) Abnormalities of floor plate, notochord and somite differentiation in the *loop-tail* (*Lp*) mouse: a model of severe neural tube defects. *Mech. Devl.*, **73**, 59–72.
30. Bilder, D. and Perrimon, N. (2000) Localization of apical epithelial determinants by the basolateral PDZ protein Scribble. *Nature*, **403**, 676–680.
31. Ybot-Gonzalez, P. and Copp, A.J. (1999) Bending of the neural plate during mouse spinal neurulation is independent of actin microfilaments. *Devl. Dyn.*, **215**, 273–283.
32. Keller, R., Shih, J. and Sater, A. (1992) The cellular basis of the convergence and extension of the *Xenopus* neural plate. *Devl. Dyn.*, **193**, 199–217.
33. Keller, R., Davidson, L., Edlund, A., Elul, T., Ezin, M., Shook, D. and Skoglund, P. (2000) Mechanisms of convergence and extension by cell intercalation. *Phil. Trans. R. Soc. Lond. B: Biol. Sci.*, **355**, 897–922.
34. Smith, L.J. and Stein, K.F. (1962) Axial elongation in the mouse and its retardation in homozygous looptail mice. *J. Embryol. Exp. Morphol.*, **10**, 73–87.
35. Wallingford, J.B., Fraser, S.E. and Harland, R.M. (2002) Convergent extension: the molecular control of polarized cell movement during embryonic development. *Devl. Cell*, **2**, 695–706.
36. Legouis, R., Gansmuller, A., Sookhareea, S., Bosher, J.M., Baillie, D.L. and Labouesse, M. (2000) LET-413 is a basolateral protein required for the assembly of adherens junctions in *Caenorhabditis elegans. Nat. Cell Biol.*, **2**, 415–422.
37. Bilder, D., Li, M. and Perrimon, N. (2002) Cooperative regulation of cell polarity and growth by *Drosophila* tumor suppressors. *Science*, **289**, 113–116.
38. Wu, L.P., Choe, K.M., Lu, Y. and Anderson, K.V. (2001) Drosophila immunity: genes on the third chromosome required for the response to bacterial infection. *Genetics*, **159**, 189–199.
39. Nakagawa, S. and Huibregtse, J.M. (2000) Human Scribble (Vartul) is targeted for ubiquitin-mediated degradation by the high-risk papillomavirus E6 proteins and the E6AP ubiquitin–protein ligase. *Mol. Cell Biol.*, **20**, 8244–8253.
40. Aaku-Saraste, E., Hellwig, A. and Huttner, W.B. (1996) Loss of occludin and functional tight junctions, but not ZO-1, during neural tube closure—remodeling of the neuroepithelium prior to neurogenesis. *Devl. Biol.*, **180**, 664–679.
41. Aaku-Saraste, E., Oback, B., Hellwig, A. and Huttner, W.B. (1997) Neuroepithelial cells downregulate their plasma membrane polarity prior to neural tube closure and neurogenesis. *Mech. Devl.*, **69**, 71–81.
42. Axelrod, J.D. (2001) Strabismus comes into focus. *Nat. Cell Biol.*, **4**, E6–E8.
43. Wodarz, A. (2001) Cell polarity: no need to reinvent the wheel. *Curr. Biol.*, **11**, R975–R978.

44. Frazzetto, G., Klingbeil, P. and Bouwmeester, T. (2002) Xenopus marginal coil (Xmc), a novel FGF inducible cytosolic coiled-coil protein regulating gastrulation movements. *Mech. Devl.*, **113**, 3–14.
45. Suzuki, N., Choe, H.R., Nishida, Y., Yamawaki-Kataoka, Y., Ohnishi, S., Tamaoki, T. and Kataoka, T. (1990) Leucine-rich repeats and carboxyl terminus are required for interaction of yeast adenylate cyclase with RAS proteins. *Proc. Natl Acad. Sci. USA*, **87**, 8711–8715.
46. Peifer, M. and Tepass, U. (2000) Which way is up? *Nature*, **403**, 611–612.
47. Harris, M.J. (2001) Why are the genes that cause risk of human neural tube defects so hard to find? *Teratology*, **63**, 165–166.
48. Nanni, L., Ming, J.E., Bocian, M., Steinhaus, K., Bianchi, D.W., De Die-Smulders, C., Giannotti, A., Imaizumi, K., Jones, K.L., Del Campo, M. *et al.* (1999) The mutational spectrum of the *Sonic Hedgehog* gene in holoprosencephaly: *SHH* mutations cause a significant proportion of autosomal dominant holoprosencephaly. *Hum. Mol. Genet.*, **8**, 2479–2488.
49. Kajiwara, K., Berson, E.L. and Dryja, T.P. (1994) Digenic retinitis pigmentosa due to mutations at the unlinked peripherin/RDS and ROM1 loci. *Science*, **264**, 1604–1608.
50. Katsanis, N., Ansley, S.J., Badano, J.L., Eichers, E.R., Lewis, R.A., Hoskins, B.E., Scambler, P.J., Davidson, W.S., Beales, P.L. and Lupski, J.R. (2001) Triallelic inheritance in Bardet-Biedl syndrome, a Mendelian recessive disorder. *Science*, **293**, 2256–2259.
51. Stanier, P., Henson, J.N., Eddleston, J., Moore, G.E. and Copp, A.J. (1995) Genetic basis of neural tube defects: the mouse gene *loop-tail* maps to a region of Chromosome 1 syntenic with human 1q21–q23. *Genomics*, **26**, 473–478.
52. Murdoch, J.N., Eddleston, J., Leblond-Bourget, N., Stanier, P. and Copp, A.J. (1999) Sequence and expression analysis of *Nhlh1*: a basic helix-loop-helix gene implicated in neurogenesis. *Devl. Genet.*, **24**, 165–177.